Biomaterials 35 (2014) 2878–2889

Contents lists available at ScienceDirect

Biomaterials

journal homepage: www.elsevier.com/locate/biomaterials

SM5-1-Conjugated PLA nanoparticles loaded with 5-fluorouracil for targeted hepatocellular carcinoma imaging and therapy

Xibo Ma [a], Zhen Cheng [b], Yushen Jin [c], Xiaolong Liang [d], Xin Yang [a], Zhifei Dai [d], Jie Tian [a,*]

[a] Key Laboratory of Molecular Imaging of Chinese Academy of Sciences, Institute of Automation, Chinese Academy of Sciences, Beijing 100190, China
[b] Molecular Imaging Program at Stanford (MIPS), Bio-X Program, Department of Radiology, Stanford University, California 94305-5344, USA
[c] Nanomedicine and Biosensor Laboratory, School of Life Science and Technology, Harbin Institute of Technology, Harbin 150080, China
[d] Department of Biomedical Engineering, College of Engineering, Peking University, Beijing, China

ARTICLE INFO

Article history:
Received 15 October 2013
Accepted 18 December 2013
Available online 8 January 2014

Keywords:
Nanoparticles
Bioluminescence imaging (BLI)
Bioluminescent tomography (BLT)
Targeted imaging and therapy

ABSTRACT

SM5-1 is a humanized mouse antibody which has a high binding specificity for a membrane protein of about 230 kDa overexpressed in hepatocellular carcinoma (HCC), melanoma and breast cancer. In this study, SM5-1-conjugated poly D, L (lactide-coglycolide) (PLA) PLA containing Cy7 (PLA-Cy7-SM5-1) was prepared to study the targeting specificity of the bioconjugate to HCC-LM3-fLuc cell. Then, SM5-1-conjugated PLA containing 5-fluorouracil (5-FU) (PLA-5FU-SM5-1) and PLA containing 5-FU (PLA-5FU) were prepared for treatment of subcutaneous HCC-LM3-fLuc tumor mice. The results showed that PLA-5FU-SM5-1, PLA-5FU and 5-FU induced a 45.07%, 23.56% and 19.05% tumor growth inhibition rate, respectively, on day 31 post-treatment as determined by bioluminescent intensity. In addition, in order to evaluate the antitumor efficacy of PLA-5FU-SM5-1, HCC-LM3-fLuc cells were injected into the liver to establish the experimental orthotopic liver tumor models. The experiments showed that PLA-5FU-SM5-1, PLA-5FU and 5-FU induced a 53.24%, 31.00%, and 18.11% tumor growth inhibition rate, respectively, on day 31 post-treatment determined by the bioluminescent intensity of the abdomen in tumor-bearing mice. Furthermore, we have calculated the three-dimensional location of the liver cancer in mice using a multilevel adaptive finite element algorithm based on bioluminescent intensity decay calibration. The reconstruction results demonstrated that PLA-5FU-SM5-1 inhibited the tumor rapid progression, which were consistent with the results of subcutaneous tumor mice experiments and *in vitro* cell experiment results.

1. Introduction

Hepatocellular carcinoma (HCC) is the second leading cause of cancer-related deaths worldwide, with the incidence on the rise [1–3]. Although many treatment options including liver transplant, surgical resection, embolization, radio embolization and chemotherapy have been developed for patients with HCC, the five-year survival rate is only approximately 26% in the United States and has not been improved significantly [3]. Population-based studies show that the incidence rate is almost equal to the death rate, indicating that most of the patients who develop HCC will die of it in the near future [1].

5-Fluorouracil (5-FU) is widely used in the treatment of a variety of tumors. It can interfere with nucleoside metabolism and result in DNA synthesis disorders and RNA dysfunction, leading to cytotoxicity and cell death [4,5]. Over the past 20 years, increased understanding of the mechanism of action of 5-FU has led to the development of many treatment strategies that improve its anticancer activity [6–8]. However, the overall response rate for many tumors to 5-FU alone remains only about 15% because of its drug resistance [9]. Therefore, new strategies, which can improve the antitumor efficacy are urgently needed [10].

A variety of nanoparticles have been used to encapsulate 5-FU in order to prolong the release time of the drug and improve accumulation concentration in the body, thereby improving the antitumor efficacy [11]. Bozkir et al. have optimized the formulation of poly D, L (lactide-coglycolide) (PLA) nanoparticles loaded with 5-FU (5FU-NP) by a nano-precipitation-solvent displacement technique. In their research, the *in vitro* release and antitumor activity of the optimized formulation with maximum drug entrapment efficiency

* Corresponding author. Tel./fax: 86 010 62527995.
E-mail address: jie.tian@ia.ac.cn (J. Tian).
URL: http://www.3dmed.net, http://www.mitk.net

0142-9612
http://dx.doi.org/10.1016/j.biomaterials.2013.12.045

and minimum particle size were examined, and the nanoparticle system was demonstrated to improve the cancer chemotherapy efficacy *in vivo* [12]. The 5-FU-colloidal gold complex (Au@5-FU) was also prepared and observed to have appreciable antitumor activity against breast cancer, colorectal cancer, leukemia, etc., which suggests that gold nanoparticles have the potential to be used as effective carriers for 5-FU [13,14]. In addition, 5-FU-loaded nanoparticles such as chitosan and polyaspartic acid sodium (CS-PAsp) and poly(ethylene glycol)-poly(γ-benzyl-L-glutamate)(PEG-PBLG) demonstrated a sustained release of 5-FU [15–17]. As carriers of antitumor drugs, PLA nanoparticles have many advantages including being non-toxic, biodegradable, avoiding uptake by the mononuclear phagocytes systems, etc. [18–21]. In addition, unlike some micron vectors, PLA nanoparticles can easily reach the target tissue and cells [22]. All of these studies suggest that 5-FU-PLA nanoparticles have high potential as anticancer agents.

The treatment of HCC patients is particularly challenging because of patient-specific, tumor-specific and liver-specific variables that impact our ability to treat patients safely and effectively [3]. Targeted drug delivery is a promising approach and an attractive field in tumor therapy. Many groups worldwide have done a lot of research on targeted therapy using some common targeting biomolecules such as anti-human epidermal growth factor receptor 2 (HER2) and Vascular Endothelial Growth Factor Receptor (VEGFR) antibodies [23–27] and have made great progress. SM5-1 is a member of a panel of humanized mouse monoclonal antibodies (mAbs) generated by using a subtractive immunization protocol as described previously [28]. SM5-1 can bind to a membrane protein of about 230 kDa (p230), which is specifically expressed in HCC, melanoma and breast cancer cells, making it a promising candidate for cancer-targeted therapy and diagnosis [29–32]. In these experiments, we found that the SM5-1 receptor was highly expressed in HCC-LM3-fLuc cells, which indicated that the SM5-1 antibody could be explored for targeted treatment of HCC (the method and data are shown in supplemental data and Fig. S1).

Optical molecular imaging including bioluminescence imaging and fluorescence imaging have drawn more and more attention due to their high sensitivity and low cost [33–36]. In recent years, they have been more and more widely used in evaluating the efficacy of antitumor drugs [37], mechanism of cancer metastasis [38–40], image protein interactions [41–46], and so on. However, two-dimensional molecular imaging cannot present accurate three-dimensional information of inner optical sources, such as in the liver, bone or lungs. Therefore, many reconstruction algorithms have been proposed such as Tikhonov regularization [47], Bone-type approximation bioluminescent tomography (BLT) method [48], a trust region method in the adaptive finite element framework [49], and the adaptive finite element method based on bioluminescent intensity decay calibration [50]. With the development of three-dimensional imaging technologies, these methods have been initially applied in the detection of optical sources in the liver and bone [50–52]. All of these studies indicated that the three-dimensional reconstruction technology could provide a powerful technique for further imaging applications.

In this paper, PLA nanoparticles loaded with 5-FU and modified with SM5-1 (represented as PLA-5FU-SM5-1) were prepared and evaluated in the treatment of liver tumors. In order to study the antitumor efficacy of PLA-5FU-SM5-1, *in vitro* cell proliferation experiments and *in vivo* animal treatment experiments were carried out using HCC-LM3-fLuc tumor models. We also reconstructed three-dimensional location information of the inner tumor using the adaptive finite elements method based on bioluminescence intensity decay calibration. Finally, the immunohistochemistry experiments were carried out to show the influence of the drug on tumor proliferation, angiogenesis and apoptosis.

2. Materials and methods

2.1. Materials and reagents

PLA (molecular weight of 80,000) was purchased from Shandong Institute of Medical Instruments (Jinan, China). The standard 5-FU (batch No. PHR1227, purity ≥99%) was purchased from Sigma Company (Shanghai, China). CellTiter 96® AQ_{UEOUS} One Solution Cell Proliferation Assay (MTS, batch No. G358A) was purchased from Promega Company (Madison, USA). Cy7 carboxylic acid (batch No. 45090) was purchased from Lumiprobe Company (Florida, USA). HCC-LM3-fLuc cells and antibody SM5-1 were kindly provided by Professor Jian Zhao and Weizhu Qian of Shanghai Second Military University respectively.

2.2. Preparation of 5-FU or Cy7 loaded PLA nanoparticles

Briefly, aqueous solution of 5-FU (150 μL) was emulsified in 1.5 mL ethyl acetate containing 40 mg PLA by sonication (15 W, 30 s). The resulting emulsion (w/o) was emulsified again by sonication (15 W, 1 min) in an aqueous solution of 1% polyvinyl alcohol to form the w/o/w double emulsion. The double emulsion was then diluted into 30 mL of 0.3% polyvinyl alcohol and the system was maintained under magnetic stirring for 8 h. The nanoparticles were collected by centrifugation at 12,000 rpm for 30 min and washed three times with deionized water by centrifugation at 12,000 rpm. Finally, the nanoparticle suspension was lyophilized at a condenser temperature of −60 °C and pressure of 5 mTorr to obtain the freeze-dried powder. Blank nanoparticles were prepared in the same procedure describe above. Cy7 encapsulated PLA nanoparticles were also prepared in the same procedure, the only difference was that Cy7 was dissolved into ethyl acetate rather than deionized water.

2.3. Preparation of SM5-1-conjugated PLA containing 5-FU (or Cy7)

Coupling of humanized SM5-1 to the PLA nanoparticle was performed using 1-ethyl-3-(3-dimethylamido-propyl) carbodiimide/N-hydroxysuccinimide (EDC/NHS) as the coupling agents. PLA nanoparticle solution (45 mg) containing 5-FU (5FU − PLA) was dissolved in 9 mL of 10 mmol/L NaH_2PO_4 (pH 6.3). This solution was activated with a mixture of NHS (0.1 mL, 50 mg/mL) and EDC (0.1 mL, 50 mg/mL) for 30 min, then antibody SM5-1 dissolved in PBS buffer (2 mL, 3.1 mg/mL, pH 7.4) was added and the reaction lasted for 4 h at room temperature. The resulting product PLA-5FU-SM5-1 was purified by washing it three times with deionized water to remove unbound antibody and was then lyophilized. Similarly, PLA-Cy7-SM5-1 was prepared with the same procedure as above.

2.4. Determination of 5-FU content and encapsulation efficiency

SM5-1 modified PLA-5FU was chosen randomly, weighed precisely with a balance and dissolved in 2 mL dichloromethane. Hydrochloric acid (HCl, 5 mL of 0.1 mol/L) was administered 3 times to extract 5-FU entirely by agitation and centrifugation (1400 ×g, 15 min × 3). The supernatant was collected and measured by a UV–Vis spectrophotometer. Repeated determinations were taken 6 times ($n = 6$). The encapsulation efficiency and loading content of 5-FU in PLA was calculated according to the following equation:

$$\text{Encapsulation efficiency}(\%) = \frac{\text{weight of drug in nanoparticles}}{\text{weight of the feeding drug}} \times 100\% \quad (1)$$

$$\text{Drug loading content}(\%) = \frac{\text{weight of drug in nanoparticles}}{\text{weight of nanoparticles}} \times 100\% \quad (2)$$

2.5. Morphological observation

The morphology of PLA-5FU-SM5-1, PLA-5FU and blank PLA nanoparticles was observed by scanning electron microscopy (SEM, Hitachi S-4300; Hitachi, Tokyo, Japan) with accelerating voltage of 15 KV. Transmission electron microscopic (TEM) images of blank PLA-5FU-SM5-1 and PLA-5FU were acquired by a Tecnai Spirit Microscope with a charge coupled device (CCD) camera operated at 80 KV.

2.6. In vitro release studies

The *in vitro* release of 5-FU was analyzed using a dialysis method [53]. Before drug release from the prepared nanoparticles, PLA-5FU-SM5-1, PLA-5FU and 5-FU were freeze-dried and the powders were re-dissolved in PBS (pH = 7.4) at a final concentration of 2 mg/mL. Each (1 mL) of the three samples at a concentration of 2 mg/mL was placed in a dialysis bag, which was immersed in a vial containing 20 mL of 10 mM PBS (pH = 7.4) and incubated while stirring at 37 °C for 120 h. A 1 mL aliquot of the release medium was withdrawn from the vial and replaced with an equal volume of fresh PBS at predetermined times. The 5-FU released from the nanoparticles was analyzed spectrophotometrically, and the solution was determined by the absorption peak intensity at 267 nm. The results were reported as mean ± SD ($n = 5$).

2.7. Cell culture

HCC-LM3-fLuc human hepatocellular carcinoma cells were grown in Dulbecco's Modified Eagle's Medium supplemented with 10% fetal bovine serum (FBS) in a humidified incubator at 37 °C in a 5% CO_2 atmosphere.

2.8. In vitro cell proliferation assay

Hepatocellular carcinoma HCC-LM3-fLuc cells were plated in four sections of 96-well plates (1×10^4 per well) and incubated overnight. The cells were then exposed to a series of concentrations of 5-FU or PLA-5FU or PLA-5FU-SM5-1 for 3 days. For three sections of the 96-well plate, cell viability was measured using a CellTiter 96 nonradioactive cell proliferation assay kit (MTS, Promega). Briefly, a 20 μL MTS solution was added to each well. After incubation for 2 h at 37 °C, the absorbance was measured at 570 nm using a BioTek Synergy HT Universal Microplate Reader. For another 96-well plate, we added PLA-5FU-SM5-1, and 20 μL of luciferin were added to each well. After incubation for 3 min at 37 °C, the bioluminescent images (BLI) were acquired using the in-house bioluminescence imaging system developed by ourselves [47,50]. The parameters of CCD (Princeton Instruments PIXIS 1024BR, Roper Scientific, USA) were set at exposure time = 2 min, f-number = 1.2, binning = 4, controller gain = 3, rate = 1 MHz, resolution = 16 bits, and readout = low noise. The experiments were carried out in a completely dark environment in order to avoid the influence of outside light.

2.9. Toxicity studies

Liver immortalized cells LO_2 were kindly provided by Dr. Xin Tong and were plated in 96-well plates (1×10^4 per well) overnight. The cells were then exposed to a series of concentrations of 5-FU or PLA-5FU or PLA-5FU-SM5-1 for 3 days. The samples were analyzed using the same procedure as described above in the section of "*In vitro cell proliferation assay*".

2.10. Animal models

Female BALB/c nude mice (4 weeks of age) were purchased from the Department of Experimental Animals, Peking University Health Science Center. All animal experiments were performed in accordance with the guidelines of the Institutional Animal Care and Use Committee at Peking University.

2.11. In vivo antitumor study based on subcutaneous live tumor mice

The HCC-LM3-fLuc tumor model was established by subcutaneous injection of 2×10^6 HCC-LM3-fLuc tumor cells into the right upper flanks of BALB/c nude mice. Antitumor activities of 5-FU, PLA-5FU and PLA-5FU-SM5-1 were determined in mice bearing the HCCs. The mice were divided into four groups and subjected to antitumor treatment when the tumor volume reached ≈100 mm^3 (about 8 days after inoculation). Four groups of HCC-LM3 tumor-bearing mice ($n = 5$ per group) were treated with saline, 5-FU, PLA-5FU-SM5-1, or PLA-5FU (10 mg 5-FU per kilogram for four consecutive days) respectively. The tumor volume was estimated, assuming the tumors were ellipsoid, using the formula volume = $4\pi/3$ (1/2 length × 1/2 width × 1/2 height). Tumor size was measured on day 0, 3, 7, 11, 15, 19, 23, 27, and 31 after treatment. In addition, we acquired the bioluminescent images of the tumor-bearing mice and calculated the bioluminescent intensity to evaluate antitumor efficacy on day 0, 3, 7, 11, 15, 19, 23, 27, and 31 respectively. The image acquisition and bioluminescent intensity calculation method were described in our previous work [37]. During the bioluminescent image acquisition, the parameters of the CCD were set the same as those of the "*In vitro cell proliferation assay*" except the binning = 1, and the experiments were carried out in a completely dark environment.

2.12. In vivo antitumor study in mice bearing the orthotopic HCC model

The orthotopic HCC mouse model was established by injecting 2×10^6 HCC-LM3-fLuc tumor cells into the liver of BALB/c nude mice. The mice were divided into four groups and subjected to antitumor treatment on the 7th day after inoculation. Four groups of orthotopic HCC tumor-bearing mice ($n = 3$ per group) were treated with saline, 5FU, PLA-5FU, or PLA-5FU-SM5-1 (10 mg 5-FU per kilogram on four consecutive days) respectively. The antitumor efficacy was evaluated on day 0, 6, 11, 16, 21, 26, and 31 by acquiring the bioluminescent images of the abdomen of the tumor-bearing mice and calculated the bioluminescent intensity. Each mouse was fasted to reduce the influence of autofluorescence for 4 h before *in vivo* BLI. The image was acquired at 8 min after intraperitoneal injection with 200 μL D-luciferin (Biotium, Inc., USA) and the parameters of CCD were set as the same as the above section. In addition, we acquired four bioluminescent images at 0°, 90°, 180°, and 270° from four mice (one mouse per group) for reconstruction of the three-dimensional bioluminescent images using the same parameters as the BLI acquisition.

2.13. Three-dimensional reconstruction of the inner source using the adaptive elements methods based on bioluminescent intensity decay calibration

Since the experiment was carried out in a totally dark environment, the propagation of bioluminescent photons in the mice tissues could be represented by the steady-state diffusion equation in BLT [54,55]. In our paper, the adaptive finite element method (FEM) based on bioluminescent intensity decay calibration was chosen to reconstruct the inner source of the mice [50]. Based on FEM, the diffusion equation could be finally transformed to:

$$\mathrm{AS}^P = \Phi^m \tag{3}$$

The three-dimensional bioluminescent sources of the four mice from the four groups were reconstructed using the above method. In order to improve the reconstruction accuracy, the mice were segmented into six major organs, including muscle, lungs, liver, spleen, heart, and bone for using the heterogeneous parameters of different tissues. The segmented CT volume data was discretized into 3246 points and 15384 tetrahedrons. To induce the ill-posedness of reconstruction, a permissible source region strategy was adopted and the permissible source region (PS) was set to:

$$\mathrm{PS} = \{(x,y,z)|12 < x < 26,\ 10 < y < 28,\ 26 < z < 42,\ (x,y,z) \in \Omega\} \tag{4}$$

In order to evaluate the antitumor efficacy, the tumor inhibition rate determined by the bioluminescent intensity could be calculated according to the following equation:

$$\frac{S_d - S_c}{S_c} \times 100\% \tag{5}$$

where S_d is the bioluminescent intensity of the PLA-5FU-SM5-1, PLA-5FU, 5-FU treated group, S_c is the bioluminescent intensity of the control group.

Meanwhile, after reconstruction, we could calculate the virtual volume (V_{virtual}) of the liver tumor located in the liver, and calculated the total volume (V_{total}) of the reconstructed tetrahedrons as well [50]. The volume of every tetrahedron was calculated by the following equation:

$$\frac{1}{6}\begin{vmatrix} x_1 & y_1 & z_1 & 1 \\ x_2 & y_2 & z_2 & 1 \\ x_3 & y_3 & z_3 & 1 \\ x_4 & y_4 & z_4 & 1 \end{vmatrix} \tag{6}$$

where (x_1, y_1, z_1), (x_2, y_2, z_2), (x_3, y_3, z_3), and (x_4, y_4, z_4) are four vertices of the tetrahedron. Then, the reconstruction accuracy determined by the location was calculated by:

$$\mathrm{RA} = \sum_{i=1}^{M} V_{\mathrm{virtual}}^{\mathrm{i}} \Big/ \sum_{j=1}^{N} V_{\mathrm{total}}^{\mathrm{j}}, \tag{7}$$

where M is the number of reconstructed tetrahedrons that are located in the liver and N is the total number of reconstructed tetrahedrons.

2.14. Immunohistochemical examination and analysis

For a histology evaluation of tumor proliferation, angiogenesis and apoptosis, PBS-treated ($n = 2$), PLA-5FU-SM5-1-treated ($n = 2$), PLA-5FU ($n = 2$) and 5-FU-treated ($n = 2$) tumors (16 days post-treatment) were excised, fixed in formalin, embedded in paraffin and cut into 3.0 μm sections for immunohistochemical staining. For tumor proliferation, a set of sections was immunostained with purified anti-MKI67 mouse monoclonal antibody (KI67, Cat. NO. TA500265, Zhongshan Jinqiao Bio-company, Beijing, China) [56]. *In situ* apoptosis assay was carried out with the Fluorescein FragEL DNA fragmentation Detection Kit (Calbiochem, San Diego, CA). Formalin-fixed paraffin sections were deparaffinized and incubated with terminal deoxynucleotidyl transferase-mediated deoxyuridine triphosphate-mediated deoxyuridine triphosphate nick-end labeling (TUNEL, QIA39) reaction mixture [57,58]. Apoptotic HCC-LM3-fLuc cells labeled with fluorescein isothiocyanate-dUTP were observed under the fluorescence microscope (Leica DFC450C). Five fields of each section (three sections of every group for the immunostain) were chosen randomly for counting the apoptosis cells and proliferation cells using the methods described in Refs. [57,58]. Tumor micro-vessel density (MVD) was quantified using sections immunostained with CD31 (BioLegend, San Diego, CA) by two investigators independently and in a blinded manner according to the method described previously [59]. The whole section was scanned at low power (×40) to determine the best fields for counting. Counting was performed on five separate fields of each section (three sections per mouse) chosen randomly at ×200 magnification. Each stained endothelial cell or cell cluster was counted as one micro-vessel. If two or more CD31-positive foci were continuous in space, this was counted as one micro-vessel. The average vessel counted from these fields in the three sections was used for MVD scoring.

2.15. Statistical analysis

Quantitative data were expressed as mean ± SD. Means were compared using one-way analysis of variance (ANOVA) and a Student t-test, and p values < 0.05 were considered statistically significant.

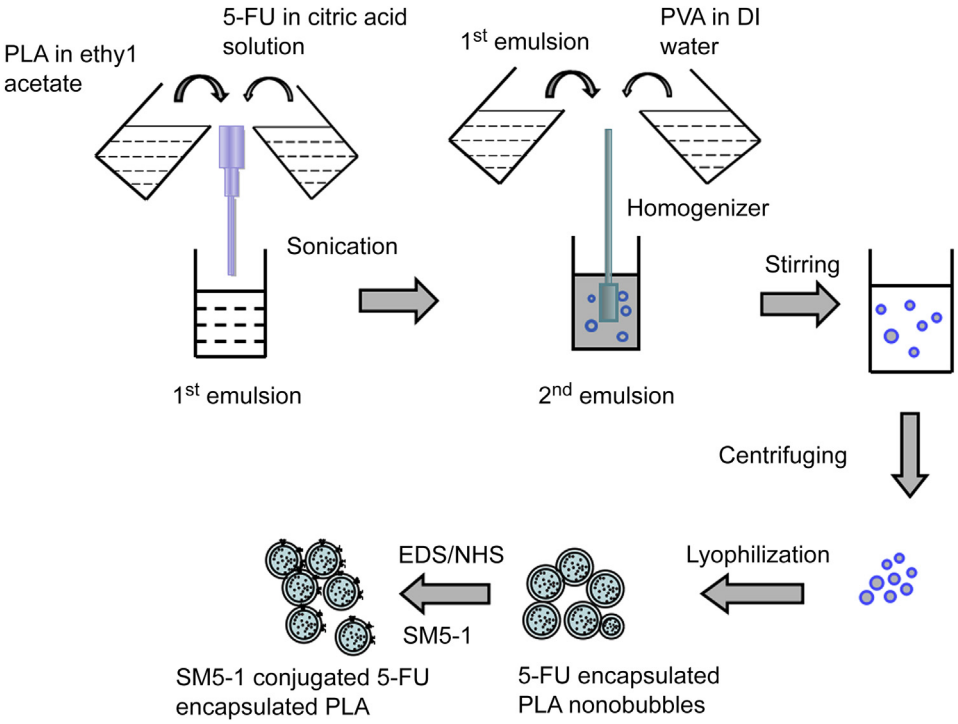

Fig. 1. Schematic illustration of the fabrication process of PLA, PLA-5FU and PLA-5FU-SM5-1.

Table 1
Properties of PLA-based drug delivery systems.

Sample	Drug loading content (%)	Encapsulation efficiency (%)
PLA-5FU	9.89 ± 0.57	8.98 ± 0.89
PLA-5FU-SM5-1	9.87 ± 0.58	8.97 ± 0.94

3. Results

3.1. Nanoparticle preparation and characterizations

Nanoparticles PLA-5FU and PLA-5FU-SM5-1 were obtained using the double nipple solvent evaporation method. The schematic illustration of the fabrication process of nanoparticles is shown in Fig. 1. It is known that PLA-based drug delivery systems usually

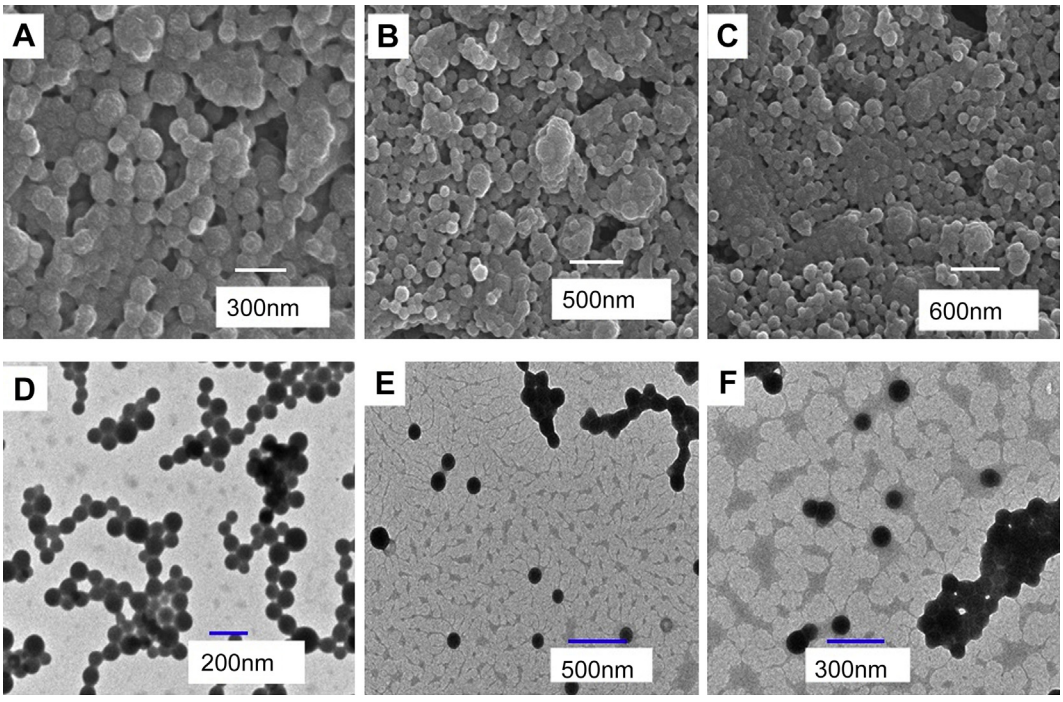

Fig. 2. SEM images of PLA (A), PLA-5FU (B) and PLA-5FU-SM5-1 (C); TEM images of PLA (D), PLA-5FU (E), and PLA-5FU-SM5-1 (F).

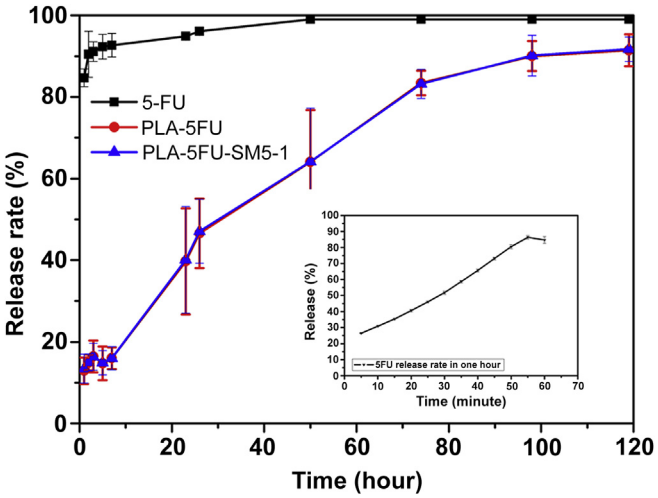

Fig. 3. *In vitro* release of 5-FU from PLA-5FU-SM5-1 (●) and vesicle-free (■) in 120 h and 5-FU release from vesicle-free in 1 h (▼) shown in the inserted figure.

have a relatively low encapsulation efficiency and drug loading (<5%) for water-soluble drugs with low molecular weights. Compared to other studies [60–62], our systems and methods showed better performance with 9.87 ± 0.58% ($n = 3$) encapsulation efficiency and 8.97 ± 0.94% drug loading, which is mainly due to the addition of excess 5-FU (shown in Table 1).

The obtained nanoparticles PLA-5FU and PLA-5FU-SM5-1 were examined by TEM and SEM. As shown in Fig. 2 A, B and C, the nanoparticles PLA, PLA-5FU and PLA-5FU-SM5-1 were spherical, and the vesicular size measured by SEM was consistent with the results measured by TEM. In addition, the nanospheres could shrink rapidly in the light during TEM scanning which are shown in Fig. 2D, E, and F. Both SEM and TEM results showed that the particle size was uniform and around 100 nm, which contributed to the characteristics of the absorption, metabolism and excretion of drugs in small animal tumor models.

3.2. In vitro drug release studies

The release profiles of 5-FU from the nanospheres are presented in Fig. 3. The release of free 5-FU from a dialysis bag (denoted as nanosphere-free) was also examined. Without nanospheres, about 84.66% of 5-FU was released from the dialysis bag in 1 h, suggesting that the use of a dialysis bag would not affect the analysis of 5-FU release from PLA over a long timescale, e.g. several tens of hours. As shown in Fig. 3, PLA released 12.95% of the encapsulated 5-FU in 1 h, and 46.58% and 83.40% of the encapsulated 5-FU in 26 h and 74 h respectively. As a result, a total of 90.00% of 5-FU was released from nanospheres in 98 h. The figure shows that 5-FU released from PLA-5FU-SM5-1 consisted of two phases: an initial burst release (in 1 h) and subsequent sustained release phase. The release profiles of PLA-5FU were consistent with those of PLA-5FU-SM5-1.

3.3. In vitro proliferation assay and toxicity studies

Fig. 4 (A and B) shows the activity of various drugs tested on HCC-LM3-fLuc and LO2 cells lines. Fig. 4C displays the bioluminescent image after different drug concentrations of PLA-5FU-SM5-1 were added to HCC-LM3-fLuc cells and incubated for 72 h. It clearly indicates (Fig. 4A) that all three drugs inhibited HCC-LM3-fLuc cell proliferation in a dose-dependent fashion, which was consistent with the results of bioluminescent imaging (Fig. 4C).

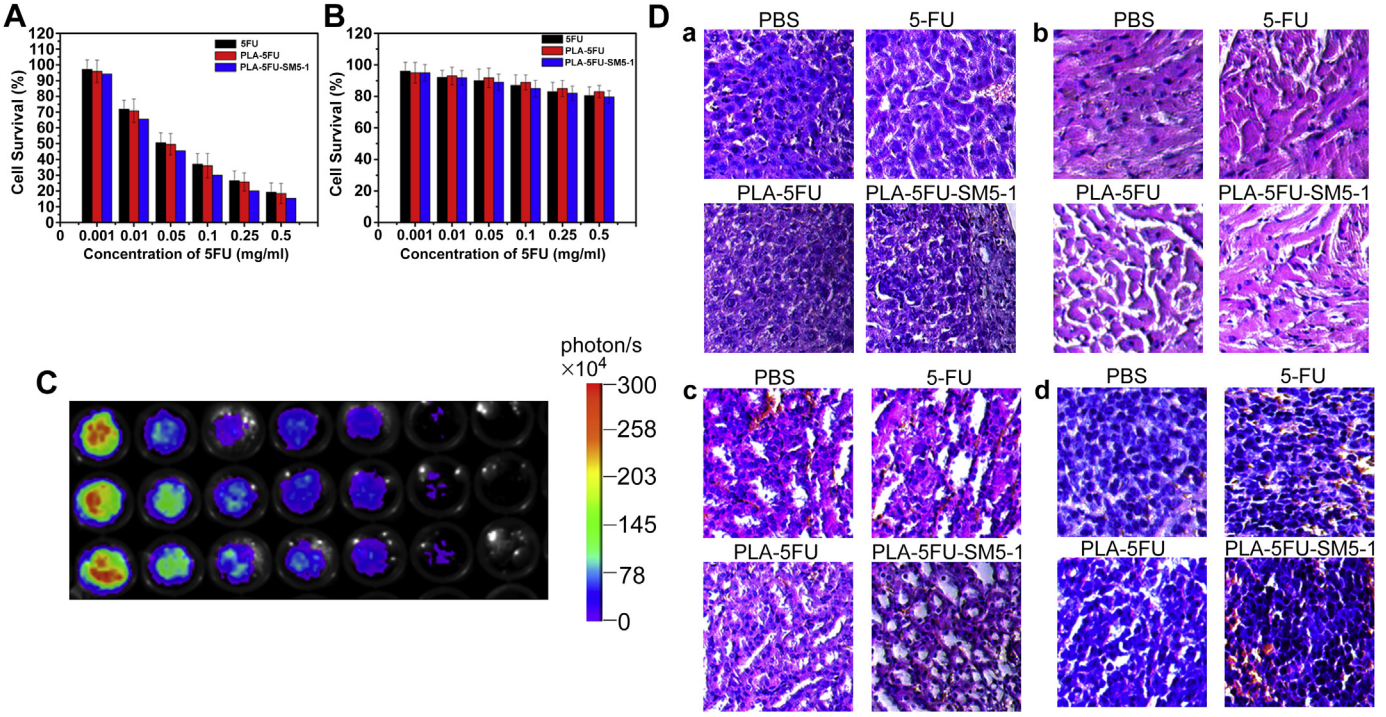

Fig. 4. (A) Anti-proliferative effects of 5-FU, PLA-5FU, and PLA-5FU-SM5-1 on HCC-LM3 cells. (B) Anti-proliferative effects of 5-FU, PLA-5FU, and PLA-5FU-SM5-1 on LO2 cells. The viability of cells was examined after 72 h exposure to different vesicles (black stands for 5-FU; red stands for PLA-5FU; blue stands for PLA-5FU-SM5-1) at different concentrations. Data shown as means ± SD ($n = 5$). (C) Bioluminescent image of anti-proliferative effects of PLA-5FU-SM5-1 on HCC-LM3 cells ($n = 3$). (D) The slide sections of the liver (a), heart (b), kidney (c) and spleen (d) stained with H&E after PBS, 5-FU, PLA-5FU and PLA-5FU-SM5-1 treatment. (For interpretation of the references to color in this figure legend, the reader is referred to the web version of this article.)

Moreover, at the same drug concentration, PLA-5FU-SM5-1 displayed higher cytotoxicity against HCC-LM3-fLuc cells as compared with PLA-5FU and 5-FU. Taking a drug concentration of 0.05 mg/mL for example, PLA-5FU-SM5-1 induced 56.4 ± 3.47% cell death *versus* PLA-5FU which induced 51.1 ± 4.32% cell death and 5-FU induced 49.8 ± 4.87% cell death. The experiments indicated that the SM5-1 antibody may lead to a higher and longer accumulation of 5-FU and thereby induce stronger cytotoxicity. Interestingly, the toxicity study of the three drugs based on LO2 cells showed that 5-FU induced more LO2 cell death in contrast to PLA-5FU and PLA-5FU-SM5-1 at the same concentration (Fig. 4B). This probably means that 5-FU has certain side effects.

In order to evaluate the toxicity of PLA-5FU-SM5-1, PLA-5FU and 5-FU *in vivo*, organs such as the heart, liver, spleen and kidneys of the mice from the four treatment groups were obtained and cut on the 16th day post-treatment, and the sections of different organs were stained with H&E. The results obtained from the fluorescence microscope images showed that the toxicity of the three drugs on the organs was not obvious except for some degree of liver damage [63,64] (Fig. 4D).

3.4. In vivo antitumor study based on a subcutaneous liver tumor

To evaluate antitumor activities of different drugs, mice were implanted subcutaneously with HCC-LM3-fLuc cells, and a therapy study was initiated when the tumor size reached about 100 mm^3 through a tail vein injection of PLA-5FU-SM5-1, PLA-5FU, 5-FU or saline. Tumor-bearing mice were treated with four doses given sequentially on day 0, 1, 2, and 3. The tumor sizes of nude mice were then measured with calipers. As shown in Figs. 5 and 6, the tumor sizes still increased in all of the four treatment groups. But interestingly, on day 7, the tumor sizes in the 5-FU treatment group were significantly smaller than those in the PLA-5FU and PLA-5FU-SM5-1 group, and the inhibition rates were 21.71 ± 3.67%, 7.74 ± 2.97%, and 18.84 ± 3.12% respectively. Afterward, the tumor sizes in the PLA-5FU-SM5-1 treated group were significantly smaller than those in the other three groups. Finally, on day 31, the inhibition rates of PLA-5FU-SM5-1, PLA-5FU and 5FU treated group were 30.69 ± 2.96, 12.54 ± 3.45 and 9.15 ± 3.45 respectively.

The baseline BLI signal was also determined on the day before the first drug administration, and then BLI was performed on day 0,

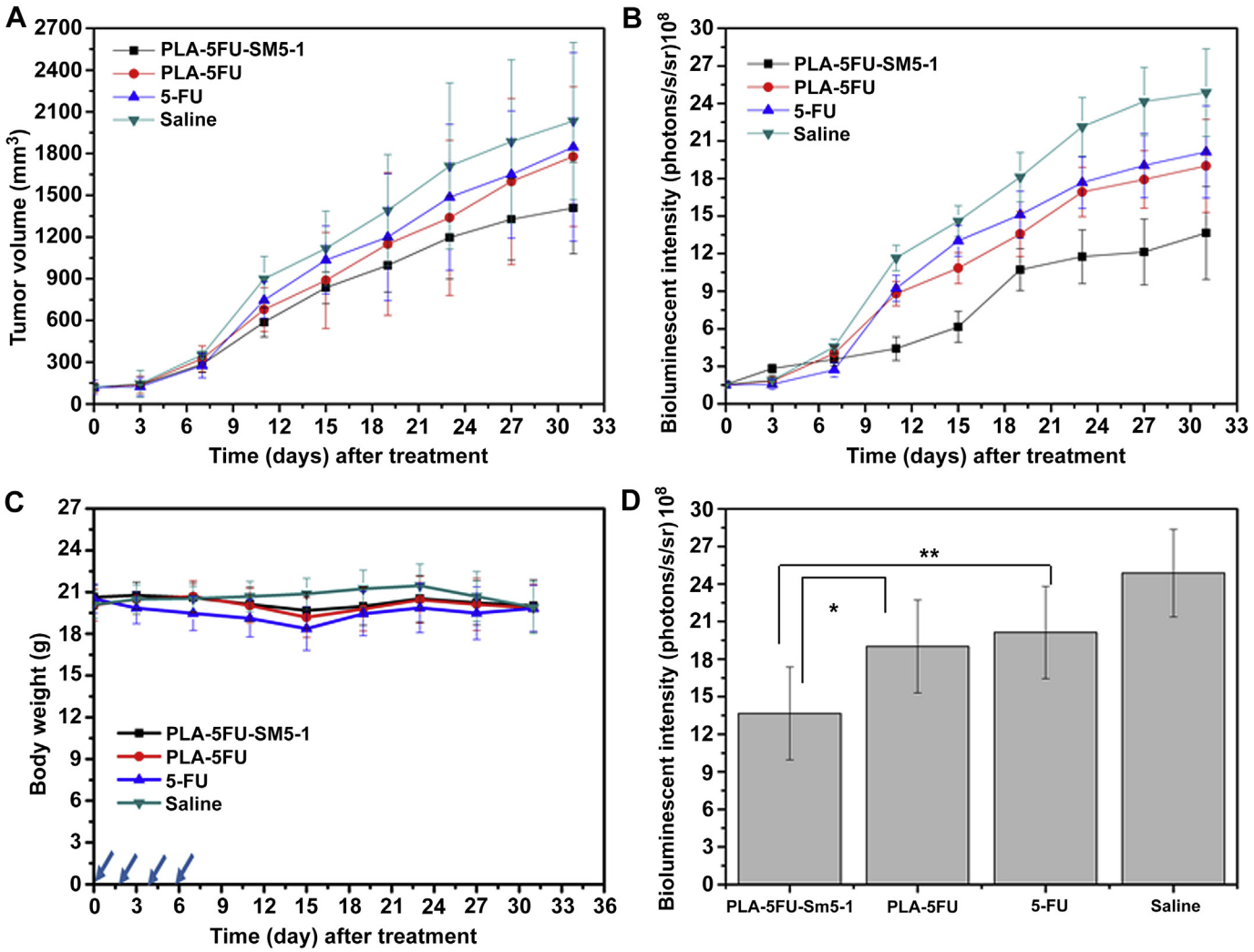

Fig. 5. (A) HCC-LM3-fLuc tumor sizes of the nude mice that underwent PLA-5FU-SM5-1, PLA-5FU, 5-FU and saline treatment. Volumes of tumors in each group were measured and expressed as a function (mean ± SD, $n = 5$ per group). (B) The quantified bioluminescent intensity of the HCC-LM3-fLuc tumors in the nude mice that underwent PLA-5FU-SM5-1, PLA-5FU, 5-FU and saline treatment. (C) The mice weight of the four groups over time ($n = 5$ per group). The drug administration intervals are indicated by *arrows*. (D) The quantitative bioluminescent intensity of the four groups on the 31st day post-treatment ($p < 0.01$, Mean ± SD, $n = 5$).

3, 7, 11, 15, 19, 23, 27, and 31 respectively to monitor the progression of the HCC-LM3-fLuc tumor burden. The presence of HCC-LM3-fLuc cells in the right flank could be clearly detected upon the intraperitoneal injection with 200 μL D-Luciferin. For the saline group, sustained tumor growth was observed (Fig. 5A and B, Fig. 6). As expected, the treatment with 5-FU, PLA-5FU, and PLA-5FU-SM5-1 clearly inhibited all tumor growth *in vivo*, although they were not able to completely ablate tumor progression. As determined by BLI (Fig. 5B and Table 3), it was found that the bioluminescent intensity of the 5-FU treatment group was the weakest among the three treatment groups, and PLA-5FU-SM5-1, PLA-5FU, and 5-FU induced a 21.88 ± 4.15%, 11.42 ± 4.32% and 40.44 ± 2.99% tumor growth inhibition rate on day 7 post-treatment respectively. Afterward, the bioluminescent intensity of the PLA-5FU-SM5-1 treatment group was obviously much weaker than that of the other three groups. From the data shown in Fig. 5 A, B and Tables 2 and 3, the antitumor efficacy determined by BLI was found to be consistent with that determined by tumor size measurement. Moreover, Fig. 5D revealed that the bioluminescent intensity of the PLA-5FU-SM5-1 treated group was much lower than that of the other two groups. The inhibition rates of the PLA-5FU-SM5-1, PLA-5FU, and 5-FU treatment groups were 45.07 ± 2.93%, 23.56 ± 3.59% and 19.05 ± 3.04% respectively on the 31st day after the first dose ($p < 0.01$).

Table 2
Inhibition rates of PLA-5FU-SM5-1, PLA-5FU, and 5-FU on HCC-LM3-fLuc tumors post-treatment determined by tumor volume.

Day after treatment	PLA-5FU-SM5-1	PLA-5FU	5-FU
7	18.84 ± 3.12**	7.74 ± 2.97	21.71 ± 3.67
11	34.56 ± 4.21#	24.47 ± 3.59	16.97 ± 4.12
15	25.32 ± 3.47##	20.58 ± 2.78	7.42 ± 2.89
19	28.40 ± 4.01*,#	17.48 ± 4.43	13.82 ± 3.75
23	30.01 ± 3.94*,##	21.77 ± 3.12	13.10 ± 3.45
27	29.65 ± 4.02**,##	15.23 ± 3.87	12.58 ± 4.23
31	30.69 ± 2.96**,##	12.54 ± 3.45	9.15 ± 3.87

* Indicates $p < 0.05$, ** indicates $p < 0.01$ (PLA-5FU-SM5-1 treated group and PLA-5FU treated group); # indicates $p < 0.05$, ## indicates $p < 0.01$ (PLA-5FU-SM5-1 treated group and 5-FU treated group).

Throughout the antitumor study, the weights of PLA-5FU-SM5-1, PLA-5FU, 5-FU and saline-treated mice were monitored (Fig. 5C). Although there was a slight loss of body weight from day 3 compared to the saline control group, none of the animals in the three drug-treated groups lost >20% of their original weight.

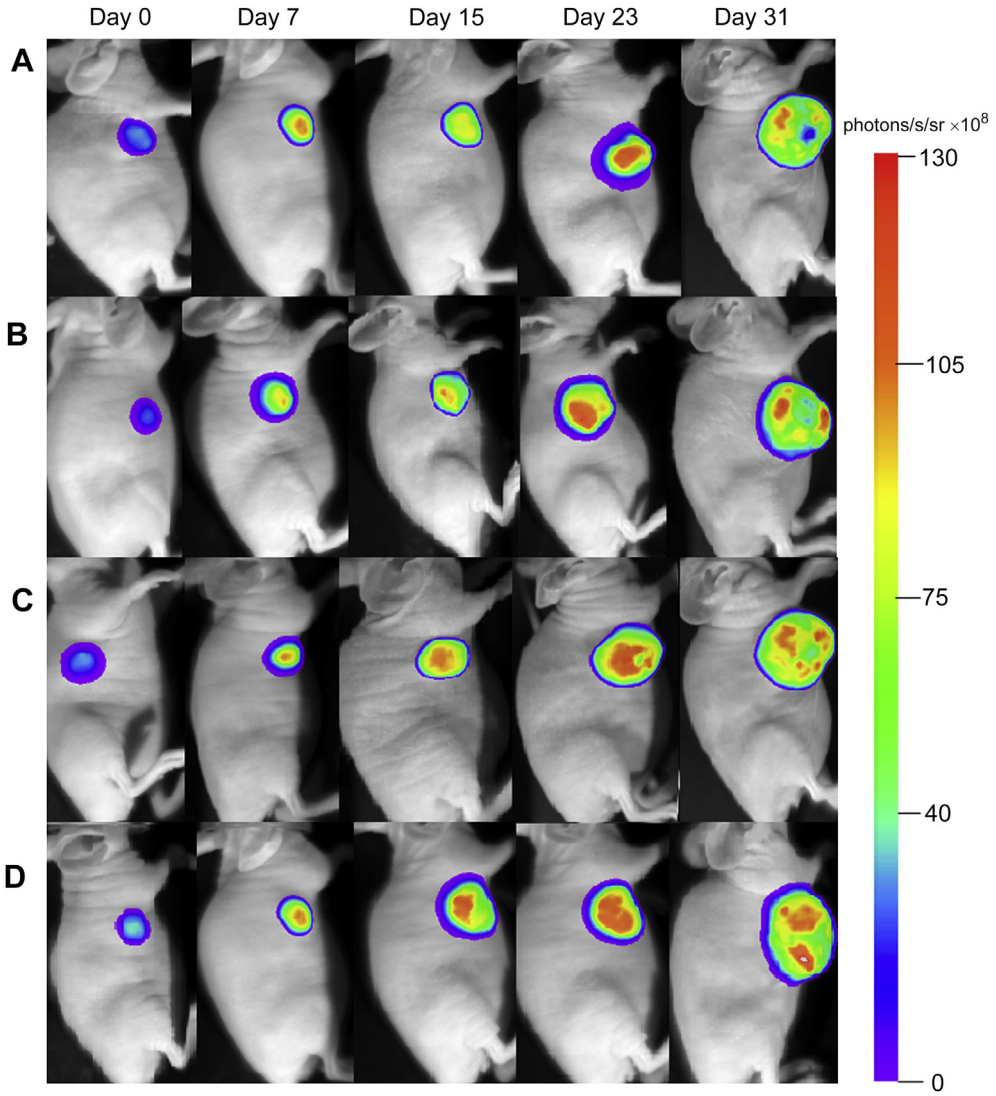

Fig. 6. Serial bioluminescent images of the HCC-LM3-fLuc tumor-bearing nude mice that underwent PLA-5FU-SM5-1 (A), PLA-5FU (B), 5-FU(C) or saline (D) treatment.

Table 3
Inhibition rate of PLA-5FU-SM5-1, PLA-5FU, and 5-FU on HCC-LM3-fLuc tumor post-treatment determined by bioluminescent intensity (BLI).

Day after treatment	PLA-5FU-SM5-1	PLA-5FU	5-FU
7	$21.88 \pm 4.15^{*,\#\#}$	11.42 ± 4.32	40.44 ± 2.99
11	$62.15 \pm 3.67^{**,\#\#}$	24.46 ± 3.87	20.77 ± 3.68
15	$57.85 \pm 4.03^{**,\#\#}$	25.70 ± 3.91	10.76 ± 4.13
19	$40.81 \pm 3.98^{**,\#\#}$	25.07 ± 3.64	16.57 ± 3.44
23	$46.86 \pm 3.95^{**,\#\#}$	23.50 ± 3.07	20.15 ± 3.81
27	$49.79 \pm 3.46^{**,\#\#}$	25.83 ± 4.14	21.19 ± 3.21
31	$45.07 \pm 2.93^{**,\#\#}$	23.56 ± 3.59	19.05 ± 3.04

* Indicates $p < 0.05$, ** indicates $p < 0.01$ (PLA-5FU-SM5-1 treated group and PLA-5FU treated group); # indicates $p < 0.05$, ## indicates $p < 0.01$ (PLA-5FU-SM5-1 treated group and 5-FU treated group).

3.5. *In vivo* antitumor study based on an orthotopic liver tumor

To evaluate antitumor activities, mice were also implanted in the liver with HCC-LM3-fLuc cells and intravenous therapy was initiated on day 7 using PLA-5FU-SM5-1, PLA-5FU, 5-FU and saline. Animals were treated with four doses given on days 0, 1, 2 and 3. The bioluminescent images of the abdomen of the tumor-bearing mice were acquired on days 0, 6, 11, 16, 21, 26 and 31 and the bioluminescent intensity of each mice could be calculated using the software Windows Molecular Imaging System (WINMI) developed by ourselves [37]. For the control group, BLI signals of the mice increased rapidly and became significantly different from the other three drug-treated groups from day 6 post-treatment (Fig. 7). As expected, 5-FU clearly inhibited tumor growth *in vivo* on the 6th day post-treatment, although tumor growth in mice from the 5-FU-treated group exceeded that of mice from the PLA-5FU-SM5-1 and PLA-5FU treated groups subsequently. Compared with the saline treated group, the tumor inhibition rates of PLA-5FU-SM5-1, PLA-5FU, and 5-FU were $53.24 \pm 3.24\%$, $31.00 \pm 3.65\%$ and $18.11 \pm 3.89\%$ respectively as determined by Equation (5) according to the bioluminescent intensity of the abdomen of tumor-bearing mice derived from WINMI (P values are all < 0.05; Fig. 7C). Moreover, it was also found that PLA-5FU-SM5-1 could effectively inhibit

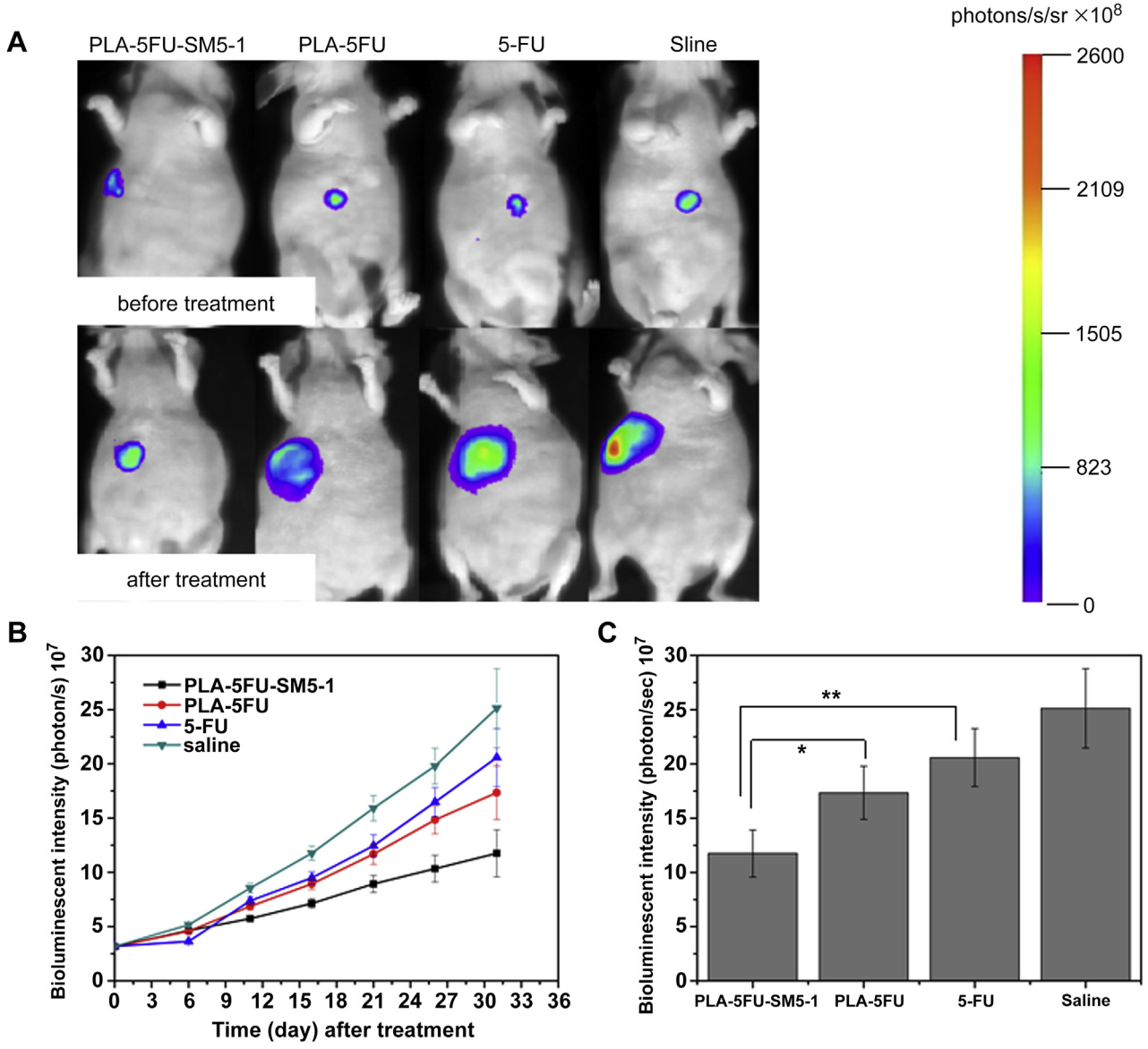

Fig. 7. (A) Bioluminescent images of orthotopic liver tumor mice from four groups on the 31st day post-treatment; (B) The quantified bioluminescent intensity of the orthotopic liver tumors that underwent PLA-5FU-SM5-1, PLA-5FU, 5-FU, and saline treatment. (C) The quantified bioluminescent intensity of tumors from the four groups on day 31 post-treatment ($p < 0.01$, mean ± SD, $n = 3$).

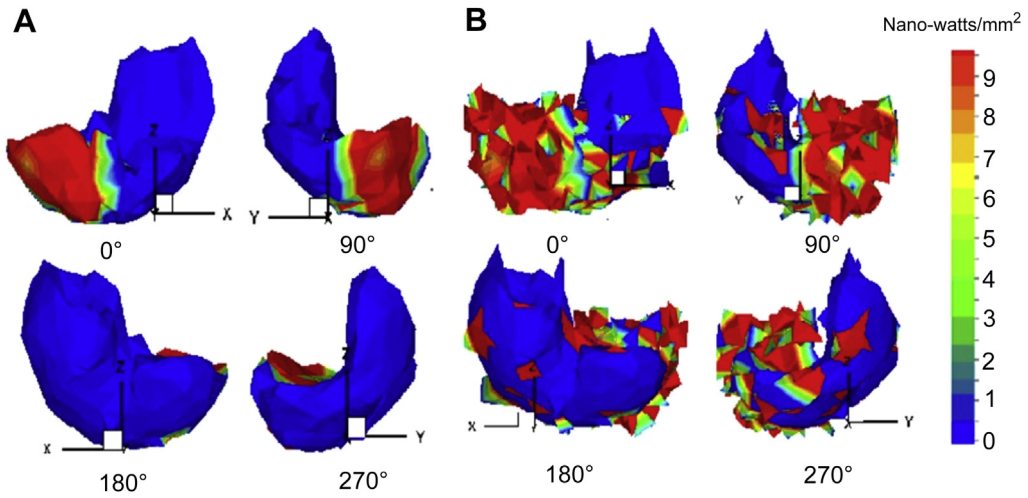

Fig. 8. Reconstruction results of a PLA-5FU-SM5-1 (A) or saline (B) treated mouse using the adaptive finite elements method based on bioluminescent intensity calibration. Four sub-figures are the reconstructed bioluminescence distribution at different angles based on the heterogeneous mouse. The dark blue (half-moon-shaped) area is the liver.(For interpretation of the references to color in this figure legend, the reader is referred to the web version of this article.)

HCC-LM3-fLuc tumor growth compared with PLA-5FU and 5-FU ($P < 0.05$; Fig. 7B).

In order to show the three-dimensional information of the orthotopic liver tumor, the BLT method was used to reconstruct the inner bioluminescence source. During reconstruction, the threshold was set at 0.5 and the regularization was set to $i \times 10^{-11}$ ($i = 1, 2, 3, 4, 5, 6, 7, 8, 9$). The reconstruction results of PLA-5FU-SM5-1 and the control group based on heterogeneous mice are shown in Fig. 8. After reconstruction, we calculated the virtual volume ($V_{virtual}$) of the liver tumor located in the liver, and calculated the total volume (V_{total}) of the reconstructed tetrahedrons as well [50]. The volume of every tetrahedron was calculated according to Equation (6) and the reconstruction accuracy was calculated by Equation (7).

The average reconstruction accuracy of the nine reconstruction results of every mouse was calculated and is shown in Table 4. The reconstructed elements (the elements where the bioluminescent intensity was greater than 70% of the maximum bioluminescent intensity were considered to be the true tumor) of PLA-5FU-SM5-1 treated mice were far fewer than those of PLA-5FU, 5-FU and saline treated group mice. According to Equations (6) and (7), the average reconstruction accuracy of the four groups was greater than 80% which demonstrated that the reconstruction results were credible for evaluating the antitumor efficacy based on orthotopic liver tumor mice models. The reconstruction figure (Fig. 8) demonstrates that PLA-5FU-SM5-1 showed higher antitumor efficacy as compared with the control saline treatment group. The quantitative reconstruction results (Table 4) showed that PLA-5FU-SM5-1, PLA-5FU, and 5-FU improved the tumor inhibition rates by 48.82 ± 4.07%, 28.89 ± 3.59% and 14.44 ± 4.32% respectively as compared with the saline treated group, which were consistent with the aforementioned results.

3.6. The effect of PLA-5FU-SM5-1 on tumor angiogenesis, apoptosis and proliferation

Data above suggested that PLA-5FU-SM5-1 could inhibit tumor proliferation and induce tumor cell apoptosis. To more rigorously demonstrate this result, HCC-LM3-fLuc xenografted tumor tissues from saline, 5-FU, PLA-5FU and PLA-5FU-SM5-1 treated mice were stained using a TUNEL assay and KI67 assay and then observed with the fluorescence microscope (shown in Fig. 9). From Fig. 9A–D, the number of apoptotic nuclei, seen as a green color under fluorescence microscopy, was greatly decreased in PLA-5FU, 5-FU or saline treated xenografts than those in PLA-5FU-SM5-1 treated xenografts. Fig. 9E–H shows that the inhibitory effects of PLA-5FU-SM5-1 on tumor growth were consistent with the results of the apoptosis study revealed by the TUNEL assay. The quantitative results (Fig. 9M and N) showed that the antitumor efficacy of PLA-5FU-SM5-1 increased about 50% than that of 5-FU. Angiogenesis is a prerequisite for advanced tumor growth and we counted the number of vessels per field to evaluate the anti-angiogenesis efficacy of the drugs. The results showed that PLA-5FU-SM5-1 could down-regulate tumor angiogenesis as compared with PLA-5FU, 5-FU and saline. Thus, all these data demonstrated PLA-5FU-SM5-1 could improve the antitumor efficacy as compared with PLA-5FU and 5-FU because of the targeting characteristics of SM5-1.

4. Discussion

Hepatocellular carcinoma HCC-LM3 is a subtype of liver cancer found in Asia with a high incidence and high death rate [58,65]. 5-FU is a common antitumor drug, which can be used in the treatment of a wide range of cancers, including colorectal, breast cancer and cancers of the digestive tract, but it has been rarely

Table 4
Reconstruction results of the four groups using the finite element method based on bioluminescent intensity calibration.

Group	Reconstruction elements (>70%)	Bioluminescent intensity (10^6photons/s)	Average reconstruction accuracy	Reconstruction times
Control	139 ± 18	6.37 ± 0.97	83.56 ± 6.75%	9
5-FU	107 ± 19	5.45 ± 0.86	84.7 ± 7.86%	9
PLA-5FU	96 ± 16	4.53 ± 0.73	83.98 ± 6.12%	9
PLA-5FU-SM5-1	89 ± 15	3.26 ± 0.64	85.12 ± 5.89%	9

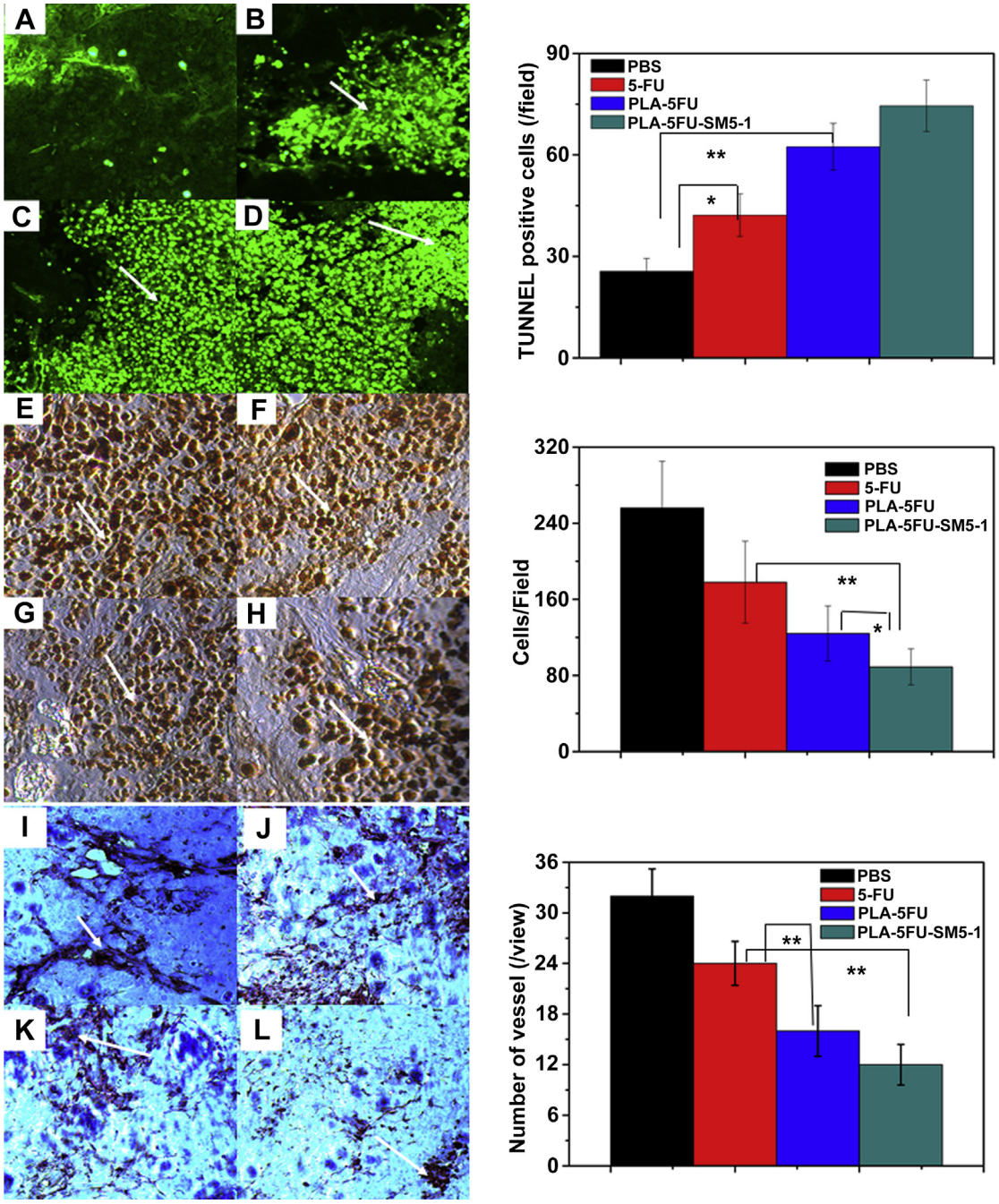

Fig. 9. Immunohistochemistry analysis of tumor cell apoptosis, cell proliferation and angiogenesis 15 days post-treatment after PBS (A, E, I), 5FU (B, F, J), PLA-5FU(C, G, K), and PLA-5FU-SM5-1 (D, H, L) treatment. Arrows indicate the apoptotic cells, proliferative cells and CD31-positive cells. M, N, and P are the quantitative results of cell apoptosis, proliferation and angiogenesis respectively.

reported to be used in the treatment of liver cancer. Moreover, the tumor inhibition rate for advanced colorectal cancer is less than 20%, which largely restricts its clinical application and treatment for other tumors [66]. We thus prepared SM5-1-conjugated PLA nanoparticles loaded with 5-FU and apply it in the treatment of HCC-LM3 cancer. Our studies demonstrate that PLA-5FU-SM5-1 nanoparticles improved the antitumor efficacy by more than 20% based on subcutaneous tumor models as compared with 5-FU and PLA-5FU. Furthermore, we found that the tumor inhibition rate was increased by more than 30% based on the orthotopic liver tumor mouse models. Then, the qualitative and quantitative results of targeted experiments showed that PLA-Cy7-SM5-1 had better targeting characteristics for orthotopic liver cancer than subcutaneous liver tumors (shown in supplemental data Fig. S2 and Table S2).

Targeted drug delivery research is an attractive field in tumor therapy. Research activity aimed towards achieving specific and targeted delivery of antitumor agents has expanded tremendously in the last several years with new avenues of directing drugs to tumors as well as new encapsulation methods of drugs [11]. Research efforts to improve chemotherapy over the past few years have led to an improvement in patient survival. However, there is a great deal more we can do to treat and perhaps prevent cancer metastasis by treating it as early as possible. PLA-5FU-SM5-1, as

demonstrated in this paper, has a prolonged circulation with 80% release of 5-FU in 72 h and it could target the tumor specifically, thereby increasing its antitumor activity while reducing its toxic side effects. This research proposed a new direction for the wide application of 5-FU.

In short, the effectiveness of the treatment was directly related to the ability to target and kill cancer cells while affecting as few healthy cells as possible. Then, how to evaluate this effectiveness was an important question too. This will require the development of superior detection methods and imaging technology [67–69]. Molecular imaging, especially optical molecular imaging, has been widely used in biological and medical research over a few years of development. However, three-dimensional bioluminescence reconstruction technologies were rarely used in cancer research and drug evaluation because of the complexity and ill-posedness of the algorithm. In this study, we obtained similar results with the traditional drug evaluation method using the adaptive finite element reconstruction method based on bioluminescent intensity decay calibration. This research clearly demonstrated the feasibility and superiority of this approach.

Future studies might focus on several directions: first of all, new therapeutic targets such as blood vessels fueling tumor growth could be developed and targeted therapeutics would be more widely used in tumor treatment; second, a set of key marker genes could be defined and used for the prospective evaluation of tumor response to 5-FU and other chemotherapeutic agents for further research; third, more rapid and convenient three-dimensional reconstruction methods should be developed to make them more widely used in drug evaluation, or even used in tumor metastasis detection; and finally, there is an urgent need for developing a multimodality molecular imaging system and calculation platform to facilitate our research in biomedical areas and pharmaceuticals development.

5. Conclusion

In this study, we prepared 5-FU-loaded PLA nanoparticles conjugated with SM5-1 (PLA-5FU-SM5-1), which exhibited favorable characteristics, including sustained drug release in an actively targeted tumor. *In vitro*, PLA-5FU-SM5-1 induced 56.4% cell death *versus* PLA-5FU, which induced 51.1% cell death and 5-FU induced 49.8% cell death. *In vivo*, PLA-5FU-SM5-1 nanoparticles showed good antitumor activity against HCC-LM3-fLuc cancer xenografts including subcutaneous tumors and orthotopic liver tumors. Meanwhile, the three-dimensional bioluminescent sources from the four treatment groups were reconstructed using the adaptive finite elements method based on bioluminescent intensity decay calibration. The statistical results of 9 reconstructions demonstrated that the tumor inhibition rate of PLA-5FU-SM5-1 was 48.80% which was consistent with the two dimensional BLI results. In addition, the *in vivo* target experiments confirmed and explained the results of the *in vivo* antitumor experiments. Taken together, our results indicated that a PLA nanoparticle delivery and antibody SM5-1 target system for 5-FU could effectively improve the therapeutic index of 5-FU and the three-dimensional reconstruction technology can provide us with a feasible method for antitumor evaluation based on inner tumor mice models.

Acknowledgments

This research was supported by the National Basic Research Program of China (973 Program) under Grant No. 2011CB707700, the National Natural Science Foundation of China under Grant Nos. 81227901, 61231004, 81071205, 81101095, 81027002, the NSFC-NIH Biomedical collaborative research program under 81261120414, the Beijing Natural Science Foundation under Grant No. 4111004, Youth Innovation Promotion Association of CAS, and the State Key Laboratory of Management and Control for Complex Systems for Youth Fund Grant No.Y3S9021F2R. The authors would also like to thank Dr. Karen M. von Deneen for the helpful revision of the manuscript.

Appendix A. Supplementary data

Supplementary data related to this article can be found at http://dx.doi.org/10.1016/j.biomaterials.2013.12.045.

References

[1] Jemal A, Bray F, Center MM, Ferlay J, Ward E, Forman D. Global cancer statistics. CA Cancer J Clin 2011;61:69–90.
[2] Siegel R, Naishadham D, Jemal A. Cancer statistics. CA Cancer J Clin 2012;62:10–29.
[3] Maluccio M, Covey A. Recent progress in understanding, diagnosing, and treating hepatocellular carcinoma. CA Cancer J Clin 2012;62:394–9.
[4] Singh UP, Ghose R, Ghose AK, Sodhi A, Singh SM, Singh RK. The effect of histidine on the structure and antitumor activity of metal-5-halouracil complexes. J Inorg Biochem 1989;37:25–39.
[5] Thomas DM, Zalcberg JR. 5-Fluorouracil: a pharmacological paradigm in the use of cytotoxics. Clin Exp Pharmacol Physiol 1998;25:887–95.
[6] Longley DB, Harkin DP, Johnston PG. 5-Fluorouracil: mechanisms of action and clinical strategies. Nat Rev Cancer 2003;3:330–8.
[7] Gramont A, Vignoud J, Tournigand C, Louvet C, Andre T, Varette C, et al. Oxaliplatin with high-dose leucovorin and 5-fluorouracil 48-hour continuous infusion in pretreated metastatic colorectal cancer. Eur J Cancer 1997;33(2):214–9.
[8] Salonga D, Danenberg KD, Johnson M, Metzger R, Groshen S, Wei DT, et al. Colorectal tumors responding to 5-fluorouracil have low gene expression levels of dihydropyrimidine dehydrogenase, thymidylate synthase, and thymidine phosphorylase. Clin Cancer Res 2000;6:1322–7.
[9] Giacchetti S, Perpoint B, Zidani R, Le Bail N, Faggiuolo R, Focan C, et al. Phase III multicenter randomized trial of oxaliplatin added to chronomodulated fluorouracilleucovorin as first-line treatment of metastatic colorectal cancer. J Clin Oncol 2000;18:136–47.
[10] Zhang N, Yin Y, Xu S, Chen W. 5-Fluorouracil: mechanisms of resistance and reversal strategies. Molecules 2008;13:1551–69.
[11] Peppas LB, Blanchette JO. Nanoparticle and targeted systems for cancer therapy. Adv Drug Deliver Rev 2012;64:206–12.
[12] Bozkir A, Saka OM. Formulation and investigation of 5-FU nanoparticles with factorial design-based studies. IL Farmaco 2005;60:840–6.
[13] Lin D, Chen H, Xue Y, Huang XJA. Bio-inspired support of gold nanoparticles-chitosan nanocomposites gel for immobilization and electrochemical study of K562 leukemia cells. Biomacromolecules 2007;8(4):1341–6.
[14] Pooja MT, Komal V, Vida AD, Shree RS. Functionalized gold nanoparticles and their biomedical applications. Nanomaterials 2011;1:31–63.
[15] Zheng Y, Yang W, Wang C, Hu J, Fu S, Dong L, et al. Nanoparticles based on the complex of chitosan and polyaspartic acid sodium salt: preparation, characterization and the use for 5-fluorouracil delivery. Eur J Pharm Biopharm 2007;67:621–31.
[16] Li S, Wang A, Jiang W, Guan Z. Pharmacokinetic characteristics and anticancer effects of 5-Fluorouracil loaded nanoparticles. BMC Cancer 2008;8:103.
[17] Wang J, Xiao B, Zheng J, Chen H, Zou S. Effect of targeted magnetic nanoparticles containing 5-FU on expression of bcl-2, bax and caspase 3 in nude mice with transplanted human liver cancer. World J Gastroentero 2007;13(23):3171–5.
[18] Bazile D, Prudhomme C, Bassoullet MT, Marlard M, Spenlehauer G, Veillard M. Stealth Me. PEG-PLA nanoparticles avoid uptake by the mononuclear phagocytes system. J Pharm SCI-US 1995;84(4):493–8.
[19] Dong YC, Feng SS. Methoxy poly (ethylene glycol)-poly (lactide) (MPEG-PLA) nanoparticles for controlled delivery of anticancer drugs. Biomaterials 2004;25(14):2843–9.
[20] Zambaux MF, Bonneaux F, Gref R, Dellacherie E, Vigneron C. Preparation and characterization of protein C-loaded PLA nanoparticles. J Control Release 1999;60(2–3):179–88.
[21] Wehrle P, Magenheim B, Benita S. The influence of process parameters on the PLA nanoparticles size distribution, evaluated by means of factorial design. Eur J Pharm Biopharm 1995;41(1):19–26.
[22] Tobio M, Gref R, Sanchez A, Langer R, Alonso MJ. Stealth PLA-PEG nanoparticles as protein carriers for nasal administration. Pharm Res-Dornr 1998;15(2):270–5.
[23] Ghobrial IM, Witzig TE, Adjei AA. Targeting apoptosis pathways in cancer therapy. CA Cancer J Clin 2005;55:178–94.
[24] Bianco R, Daniele G, Ciardiello F, Tortora G. Monoclonal antibodies targeting the epidermal growth factor receptor. Curr Drug Targets 2005;6:275–87.

[25] Emens LA. Trastuzumab: targeted therapy for the management of HER-2/neu-overexpressing metastatic breast cancer. Am J Ther 2005;12:243–53.
[26] Marty M, Cognetti F, Maraninchi D, Snyder R, Mauriac L, Hulin MT, et al. Randomized phase II trial of the efficacy and safety of trastuzumab combined with docetaxel in patients with human epidermal growth factor receptor 2-positive metastatic breast cancer administered as first-line treatment: the M77001 study group. J Clin Oncol 2005;23:4265–74.
[27] Qu Z, Griffiths GL, Wegener WA, Chang CH, Govindan SV, Horak ID, et al. Development of humanized antibodies as cancer therapeutics. Methods 2005;36:84–95.
[28] Trefzer U, Rietz N, Chen Y, Audring H, Herberth G, Siegel P, et al. SM5-1: a new monoclonal antibody which is highly sensitive and specific for melanocytic lesions. Arch Dermatol Res 2000;292:583–9.
[29] Wang H, Song S, Kou G, Li BH, Zhang DP, Hou S, et al. Treatment of hepatocellular carcinoma in a mouse xenograft model with an immunotoxin which is engineered to eliminate vascular leak syndrome. Cancer Immunol Immunother 2007;56:1775–83.
[30] Li BH, Wang H, Zhang DP, Qian WZ, Hou S, Shi S, et al. Construction and characterization of a high-affinity humanized SM5-1 monoclonal antibody. Biochem Biophys Res Commun 2007;357:951–6.
[31] Dai J, Jin J, Li B, Wang H, Hou S, Qian W, et al. A chimeric SM5-1 antibody inhibits hepatocellular carcinoma cell growth and induces caspase-dependent apoptosis. Cancer Lett 2007;258:208–14.
[32] Gao J, Kou G, Chen H, Wang H, Li BH, Lu Y, et al. Treatment of hepatocellular carcinoma in mice with PE38KDEL type I mutant-loaded poly(lactic-co-glycolic acid) nanoparticles conjugated with humanized SM5-1 F(ab′) fragments. Mol Cancer Ther 2008;7:3399–407.
[33] Willmann J, Bruggen N, Dinkelborg L, Gambhir S. Molecular imaging in drug development. Nature 2008;7:591–606.
[34] Weissleder R, Ntziachristos V. Shedding light onto live molecular targets. Nat Med 2003;9:123–8.
[35] Ntziachristos V, Ripoll J, Wang LHV, Weissleder R. Looking and listening to light: the evolution of whole body photonic imaging. Nat Biotechnol 2005;23:313–20.
[36] Weissleder R, Pittet MJ. Imaging in the era of molecular oncology. Nature 2008;452:580–9.
[37] Ma X, Liu Z, Gao QJ, Yang X, Tian J, Wang F, et al. Dual-modality monitoring of tumor response to cyclophosphamide therapy in mice with bioluminescence imaging and small-animal positron emission tomography. Mol Imaging 2011;10(4):278–83.
[38] Weissleder R. Molecular imaging in cancer. Science 2006;312:1168–71.
[39] Orlova A, Tolmachev V, Pehrson R, Lindborg M, Tran T, Sandström M, et al. Synthetic affibody molecules: a novel class of affinity ligands for molecular imaging of HER2-Expressing malignant tumors. Cancer Res 2007;67(5):2178–85.
[40] Goetz M, Ziebart A, Foersch S, Vieth M, Waldner MJ, Delaney P, et al. In vivo molecular imaging of colorectal cancer with confocal endomicroscopy by targeting epidermal growth factor receptor. Gastroenterology 2010;138:435–46.
[41] Paulmurugan R, Gambhir S. Monitoring protein–protein interactions using split synthetic renilla luciferase protein fragment assisted complementation. Anal Chem 2003;75:1584–9.
[42] Luker K, Smith M, Luker G, Gammon S, Piwnica-Worms H, Piwnica-Worms D. Kinetics of regulated protein-protein interactions revealed with firefly luciferase complementation imaging in cells and living animals. P Natl Acad Sci U S A 2004;101:12288–93.
[43] Remy I, Michnick S. A highly sensitive protein-protein interaction assay based on Gaussia luciferase. Nat Methods 2006;3:977–9.
[44] Villalobos V, Naik S, Worms DP. Current state of imaging protein-protein interactions in vivo with genetically encoded receptors. Biomed Eng Online 2007;9:321–49.
[45] Xu XD, Soutto M, Xie Q, Servick S, Subramanian C, Arnim AG, et al. Imaging protein interactions with bioluminescence resonance energy transfer (BRET) in plant and mammalian cells and tissues. P Natl Acad Sci U S A 2007;104(24):10264–9.
[46] Massoud TF, Paulmurugan R, De A, Ray P, Gambhir SS. Reporter gene imaging of protein–protein interactions in living subjects. Curr Opin Biotech 2007;18:31–7.
[47] Lv Y, Tian J, Cong W, Wang G, Luo J, Yang W, et al. A multilevel adaptive finite element algorithm for bioluminescence tomography. Opt Express 2006;14:8211–23.
[48] Cong W, Durairaj K. A born-type approximation method for bioluminescence tomography. Med Phys 2006;33:679–86.
[49] Zhang B, Yang X, Qin C, Liu D, Zhu S, Feng J, et al. A trust region method in adaptive finite element framework for bioluminescence tomography. Opt Express 2010;18:6477–91.
[50] Ma X, Tian J, Qin C, Yang X, Zhang B, Xue Z, et al. Early detection of liver cancer based on bioluminescence tomography. Appl Optics 2011;50(10):1389–95.
[51] Ma X, Deng K, Zhu S, Qin C, Liu X, Xue Z, et al. Novel registration for micro-CT and bioluminescence imaging based on iterated optimal projection. J Biomed Opt 2013;18(2):026013.
[52] Corlu A, Choe R, Durduran T, Rosen MA, Schweiger M, Arridge SR, et al. Three-dimensional in vivo fluorescence diffuse optical tomography of breast cancer in humans. Opt Express 2007;15(11):6696–716.
[53] Chidambaram N, Burgess DJ. A novel in vitro release method for submicron sized dispersed systems. AAPS Pharm Sci 1999;1(3):E11.
[54] Cong W, Wang G, Kumar D, Liu Y, Jiang M, Wang LV, et al. Practical reconstruction method for bioluminescence tomography. Opt Express 2005;13(18):6756–71.
[55] Schweiger M, Arridge SR, Hiraoka M, Delpy DT. The finite element method for the propagation of light in scattering media; boundary and source conditions. Med Phys 1995;22(11):1779–92.
[56] Leyton J, Latigo JR, Perumal M, Dhaliwal H, He Q, Aboagye EO. Early detection of tumor response to chemotherapy by 3′-deoxy-3′-[18F] fluorothymidine positron emission tomography: the effect of cisplatin on a fibrosarcoma tumor model *in vivo*. Cancer Res 2005;65(10):4202–10.
[57] Tong X, Li K, Luo Z, Lu B, Liu X, Wang T, et al. Decreased TIP30 expression promotes tumor metastasis in lung cancer. Am J Pathol 2009;174(5):1931–9.
[58] Zhao J, Dong L, Lu B, Wu G, Xu D, Chen J, et al. Down regulation of osteopontin suppresses growth and metastasis of hepatocellular carcinoma via induction of apoptosis. Gastroenterology 2008;135:956–68.
[59] Weidner N, Semple JP, Welch WR, Folkman J. Tumor angiogenesis and metastasis – correlation in invasive breast carcinoma. N Engl J Med 1991;324:1–8.
[60] Arica B, Calis S, Kas HS, Sargon MF, Hincal AA. 5-Fluorouracil encapsulated alginate beads for the treatment of breast cancer. Int J Pharmaceut 2002;242:267–9.
[61] Shantha KL, Harding DRK. Preparation and in-vitro evaluation of poly[N-vinyl-2-pyrrolidone-polyethylene glycol diacrylate]-chitosan interpolymeric pH-responsive hydrogels for oral drug delivery. Int J Pharmaceut 2000;207:65–70.
[62] Antonietti M, Forster S. Vesicles and liposomes: a self-assembly principle beyond lipids. Adv Mater 2003;15:1323–33.
[63] Schwab M, Zanger UM, Marx C, Schaeffeler E, Klein K, Dippon J, et al. Role of genetic and nongenetic factors for fluorouracil treatment-related severe toxicity: a prospective clinical trial by the german 5-FU toxicity study group. J Clin Oncol 2008;26(13):2131–8.
[64] Gamelin BE, Celle MB, Meyer GV, Delva R, Lortholary A, Genevieve F, et al. Correlation between uracil and dihydrouracil plasma ratio, Fluorouracil (5-FU) pharmacokinetic parameters, and tolerance in patients with advanced colorectal cancer: a potential interest for predicting 5-FU toxicity and determining optimal 5-FU dosage. J Clin Oncol 1999;17:1105–10.
[65] Zhao J, Lu B, Xu H. Thirty-kilodalton Tat-interacting protein suppresses tumor metastasis by inhibition of osteopontin transcription in human hepatocellular carcinoma. Hepatology 2008;48:265–75.
[66] Johnston PG, Kaye S. Capecitabine: a novel agent for the treatment of solid tumors. Anti-Cancer Drug 2001;12:639–46.
[67] Cai W, Rao J, Gambhir SS, Chen X. How molecular imaging is speeding up antiangiogenic drug development. Mol Cancer Ther 2006;5:2624–33.
[68] Savariar EN, Felsen CN, Nashi N, Jiang T, Ellies LG, Steinbach P, et al. Real-time in vivo molecular detection of primary tumors and metastases with ratiometric activatable cell-penetrating peptides. Cancer Res 2013;73(2):855–64.
[69] Baum RP, Prasad V, Muller D, Schuchardt C, Orlova A, Wennborg A, et al. Molecular imaging of her2-expressing malignant tumors in breast cancer patients using synthetic ^{111}In-or ^{68}Ga-labeled affibody molecules. J Nucl Med 2010;51:892–7.